A large strain thermodynamically-based viscoelastic-viscoplastic model applied to two-dimensional finite element analysis of solids

Péricles R. P. Carvalho[1], Humberto B. Coda[1], Rodolfo A. K. Sanches[1]

[1]*Dept. of Structural Engineering, São Carlos School of Engineering, University of São Paulo*
Av. Trab. São Carlense, 13566-590, São Carlos, São Paulo, Brazil
periclescarvalho@usp.br, hbcoda@sc.usp.br, rodolfo.sanches@usp.br

Abstract. In this work, we propose a large strain viscoelastic-viscoplastic constitutive model applied to two-dimensional finite element analysis of solids. The model is developed in a thermodynamic framework, based on the multiplicative decomposition of the deformation gradient into elastic, viscous and plastic components. The viscoelastic part is represented by Zener's rheological model, and is formulated with an internal variable approach, with evolution law in terms of the viscous deformations gradient rates. For the viscoplastic part, we apply a Perzyna-like model, including a large strain generalization of the classical Armstrong-Frederick kinematic hardening. In order to characterize the proposed constitutive model, we present results of uniaxial relaxation and creep tests under different analysis conditions, as well as more complex examples showing the potentialities of the developed framework.

Keywords: Large strain, viscoelastic, viscoplastic, finite element method

1 Introduction

Viscoelastic-viscoplastic materials are known for exhibiting rate-dependent behaviour both in the elastic and plastic stages, as shown in experimental results such as [1, 2] for polymeric materials and [3] for asphalt. In the context of large strain models, some of the earlier works is due to [4, 5], who proposes two different methods of coupling viscoelastic and viscoplastic effects, and [6], who developed a generalized constitutive modelling framework. For a more detailed state of the art review in that regard, one can refer to [7].

In this work, we present a thermodynamically-based viscoelastic-viscoplastic constitutive law based on the rheological model shown in Fig. 1, and using the concept of multiplicative decomposition [8, 9], commonly adopted in large strain formulations. The viscoelastic part is represented by a Zener model [10, 11], while the viscoplastic part is represented by a slider, connected in parallel with a rate-dependent component reproducing the Perzyna model [12], and a kinematic hardening component reproducing the Armstrong-Frederick model [13, 14].

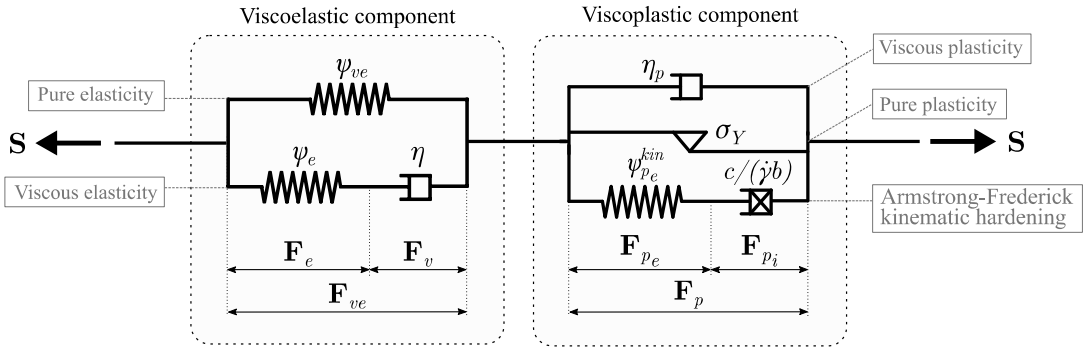

Figure 1. Rheological model

2 Kinematics

Based on Fig. 1, we assume that the total deformation gradient ($\mathbf{F}$) can be split into a viscoelastic part ($\mathbf{F}_{ve}$) and a plastic/viscoplastic part ($\mathbf{F}_p$). Furthermore, the viscoelastic part can be split into a purely elastic part ($\mathbf{F}_e$) and a viscous part ($\mathbf{F}_v$), and the plastic deformation can be split into a plastic-elastic ($\mathbf{F}_{p_e}$) and a plastic-inelastic part ($\mathbf{F}_{p_i}$). By using the multiplicative decomposition, originally introduced by [8, 9] in the context of elastoplasticity, we can express the total deformation gradient as

$$\mathbf{F} = \mathbf{F}_{ve}\mathbf{F}_p = \mathbf{F}_e\mathbf{F}_v\mathbf{F}_{p_e}\mathbf{F}_{p_i}. \tag{1}$$

For each generic component $\mathbf{F}_{(\cdot)}$ of the deformation gradient, one can define its associated components of: Jacobian as $J_{(\cdot)} = \det \mathbf{F}_{(\cdot)}$; right Cauchy-Green stretch tensor as $\mathbf{C}_{(\cdot)} = \mathbf{F}_{(\cdot)}^T\mathbf{F}_{(\cdot)}$; Green-Lagrange strain tensor as $\mathbf{E}_{(\cdot)} = \frac{1}{2}\left(\mathbf{C}_{(\cdot)} - \mathbf{I}\right)$; velocity gradient as $\mathbf{L}_{(\cdot)} = \dot{\mathbf{F}}_{(\cdot)}\mathbf{F}_{(\cdot)}^{-1}$; and deformation rate as $\mathbf{D}_{(\cdot)} = \text{sym}\left(\mathbf{L}_{(\cdot)}\right) = \frac{1}{2}\left(\mathbf{L}_{(\cdot)} + \mathbf{L}_{(\cdot)}^T\right) = \mathbf{F}_{(\cdot)}^{-T}\dot{\mathbf{E}}_{(\cdot)}\mathbf{F}_{(\cdot)}^{-1}$.

3 Thermodynamics framework

The present constitutive model is thermodynamically-based, meaning that it is derived from the second law of thermodynamics, expressed in this work as the isothermal Clausius-Duhem inequality $d_{int} = \mathbf{S} : \dot{\mathbf{E}} - \dot{\psi} \geq 0$, where d_{int} is the internal dissipation, $\mathbf{S}$ is the second Piola-Kirchhoff Stress and ψ is the Helmholtz free energy. The latter can be taken as the sum of the four spring components represented in Fig. 1, each written in terms of their respective strain components. Therefore, we can write

$$\psi = \psi_{ve}(\mathbf{E}_{ve}) + \psi_e(\mathbf{E}_e) + \psi_{p_e}^{kin}(\mathbf{E}_{p_e}), \tag{2}$$

$$\dot{\psi} = \frac{\partial \psi_{ve}}{\partial \mathbf{E}_{ve}} : \dot{\mathbf{E}}_{ve} + \frac{\partial \psi_e}{\partial \mathbf{E}_e} : \dot{\mathbf{E}}_e + \frac{\partial \psi_{p_e}^{kin}}{\partial \mathbf{E}_{p_e}} : \dot{\mathbf{E}}_{p_e}, \tag{3}$$

In this work, we assume that ψ_{ve}, ψ_e and $\psi_{p_e}^{kin}$ are isotropic. After performing certain algebraic manipulations using eq. (3) and the kinematic relations in section 2, the Clausius-Duhem inequality can be written as

$$\begin{aligned} d_{int} = \quad & \left(\mathbf{S} - \mathbf{F}_p^{-1}\frac{\partial \psi_{ve}}{\partial \mathbf{E}_{ve}}\mathbf{F}_p^{-T} - \mathbf{F}_p^{-1}\mathbf{F}_v^{-1}\frac{\partial \psi_e}{\partial \mathbf{E}_e}\mathbf{F}_v^{-T}\mathbf{F}_p^{-T}\right) : \dot{\mathbf{E}} + \left(\mathbf{C}_e\frac{\partial \psi_e}{\partial \mathbf{E}_e}\right) : \mathbf{L}_v \\ & + \left(\mathbf{C}_{ve}\frac{\partial \psi_{ve}}{\partial \mathbf{E}_{ve}} + \mathbf{F}_v^T\mathbf{C}_e\frac{\partial \psi_e}{\partial \mathbf{E}_e}\mathbf{F}_v^{-T} - \mathbf{F}_{p_e}\frac{\partial \psi_{p_e}^{kin}}{\partial \mathbf{E}_{p_e}}\mathbf{F}_{p_e}^T\right) : \mathbf{L}_p + \left(\mathbf{C}_{p_e}\frac{\partial \psi_{p_e}^{kin}}{\partial \mathbf{E}_{p_e}}\right) : \mathbf{L}_{p_i} \geq 0 \end{aligned} \tag{4}$$

From the arbitrarity of $\dot{\mathbf{E}}$, the non-negativeness of the first term in ineq. (4) can be achieved by setting the second Piola-Kirchhoff stress as

$$\mathbf{S} = \mathbf{F}_p^{-1}\frac{\partial \psi_{ve}}{\partial \mathbf{E}_{ve}}\mathbf{F}_p^{-T} + \mathbf{F}_p^{-1}\mathbf{F}_v^{-1}\frac{\partial \psi_e}{\partial \mathbf{E}_e}\mathbf{F}_v^{-T}\mathbf{F}_p^{-T}, \tag{5}$$

and the Clausius-Duhem inequality can be written simply as

$$d_{int} = \mathbf{M}_e : \mathbf{L}_v + \mathbf{\Sigma} : \mathbf{L}_p + \mathbf{M}_p : \mathbf{L}_{p_i} \geq 0 \tag{6}$$

where $\mathbf{\Sigma}$ is called relative stress, and the tensors $\mathbf{M}_{(\cdot)}$ are Mandel-like stress measures, defined, respectively, by

$$\mathbf{\Sigma} = \mathbf{M}_{ve} + \mathbf{F}_v^T\mathbf{M}_e\mathbf{F}_v^{-T} - \mathbf{F}_{p_e}\frac{\partial \psi_{p_e}^{kin}}{\partial \mathbf{E}_{p_e}}\mathbf{F}_{p_e}^T, \tag{7}$$

$$\mathbf{M}_e = \mathbf{C}_e\frac{\partial \psi_e}{\partial \mathbf{E}_e}, \qquad \mathbf{M}_{ve} = \mathbf{C}_{ve}\frac{\partial \psi_{ve}}{\partial \mathbf{E}_{ve}}, \qquad \text{and} \qquad \mathbf{M}_p = \mathbf{C}_{p_e}\frac{\partial \psi_{p_e}^{kin}}{\partial \mathbf{E}_{p_e}}. \tag{8}$$

4 Evolution laws

In order to fulfill the Clausius-Duhem inequality, one must set appropriate expressions for $\mathbf{L}_v$, $\mathbf{L}_p$ and $\mathbf{L}_{p_i}$, known as evolution laws. For $\mathbf{L}_v$, we apply the viscous evolution equation of [10] and [11]. For $\mathbf{L}_p$, a finite strain generalization of the Perzyna model [12] is used. Finally, for $\mathbf{L}_{p_i}$, the Armstrong-Frederick kinematic hardening model discussed in [13, 14] is applied. By taking into account the kinematic relation $\mathbf{L}_{(\cdot)} = \dot{\mathbf{F}}_{(\cdot)}\mathbf{F}_{(\cdot)}^{-1}$, we can also write the evolution laws in terms of the rates of deformation gradients, resulting in

$$\mathbf{L}_v = \frac{1}{\eta}\mathbf{M}_e^D \qquad \Rightarrow \qquad \dot{\mathbf{F}}_v = \frac{1}{\eta}\mathbf{M}_e^D\mathbf{F}_v, \tag{9}$$

$$\mathbf{L}_p = \frac{\langle\Theta\rangle}{\eta_p}\frac{\boldsymbol{\Sigma}^D}{\|\boldsymbol{\Sigma}^D\|} \qquad \Rightarrow \qquad \dot{\mathbf{F}}_p = \frac{\langle\Theta\rangle}{\eta_p}\frac{\boldsymbol{\Sigma}^D}{\|\boldsymbol{\Sigma}^D\|}\mathbf{F}_p, \tag{10}$$

$$\mathbf{L}_{p_i} = \frac{\langle\Theta\rangle}{\eta_p}\frac{b}{c}\mathbf{M}_p^D \qquad \Rightarrow \qquad \dot{\mathbf{F}}_{p_i} = \frac{\langle\Theta\rangle}{\eta_p}\frac{b}{c}\mathbf{M}_p^D\mathbf{F}_{p_i}, \tag{11}$$

where η is the viscosity parameter, η_p is the plastic viscosity, c is the hardening stiffness, b is a dimensionless Armstrong-Frederick parameter, and Θ is the so-called overstress of the Perzyna model. The superscript $(\cdot)^D$ denotes the deviatoric part of a tensor, $\|\cdot\|$ denotes the norm, and $\langle\cdot\rangle$ denotes the Macauley brackets.

The overstress (Θ) is expressed in terms of the yield function (Φ), and needs to be continuous and convex for positive values of Φ, and return zero when $\Phi = 0$ [15]. In the present model, the overstress function is given by Norton's rule [16]: $\Theta = (\Phi/\alpha_p)^m$, where α_p and m are calibration parameters. Furthermore, Φ is defined by a von Mises yield criterion, i.e. $\Phi = \|\boldsymbol{\Sigma}^D\| - \sqrt{2/3}\sigma_Y$, where σ_Y is the yield stress of the material.

By applying the evolution laws (9), (10) and (11) into ineq. (6), one can easily prove that the Clausius-Duhem inequality holds. Furthermore, it is possible to verify that the adopted formulation fulfils the property of inelastic incompressibility, i.e. the inelastic Jacobians J_v, J_p and J_{p_i} are constant and equal to 1.

5 Numerical implementation

The numerical application of the proposed constitutive model is performed by means of an viscoelastic prediction and viscoplastic correction algorithm. The time integration method applied in the evolution equations (9)-(11) is the backward Euler method, which is advantageous for its simplicity, but has the disadvantage of producing errors regarding the property of inelastic incompressibility, as shown in further analyses. The resulting system of equations for the evolution laws is nonlinear, solved in this work by the Newton-Raphson procedure. For the components of Helmholtz free energy, we apply a neo-Hookean law, written in each case as follows:

$$\psi_{ve} = \frac{\Lambda}{2}(\ln J_{ve})^2 + \mu_{ve}\left(\operatorname{tr}\mathbf{E}_{ve} - \ln J_{ve}\right), \tag{12}$$

$$\psi_e = \mu_e\left(\operatorname{tr}\mathbf{E}_e - \ln J_e\right), \quad \text{and} \tag{13}$$

$$\psi_{p_e}^{kin} = \frac{c}{2}\left(\operatorname{tr}\mathbf{E}_{p_e} - \ln J_{p_e}\right). \tag{14}$$

where Λ, μ_e, μ_{ve} are the Lamé parameters of the material, and c is already defined in the eq. (11).

6 Uniaxial relaxation and creep tests

In order to characterize the basic constitutive behaviour of the present model, we begin our analysis with simple uniaxial examples of relaxation and creep, using the material parameters shown in Table 1.

Table 1. Material parameters

Λ (MPa)	μ_{ve} (MPa)	μ_e (MPa)	η (MPa·s)	σ_Y (MPa)	c (MPa)	b	η_p (s)	α_p (MPa)	m
320	80	40	50	35	100	2.7	1	35	1

For the relaxation test, we apply prescribed tensile engineering strain, evolving linearly from 0 to 0.5 up until the time instant t_1 ('loading' stage), and fixed in 0.5 from t_1 to t_2 ('relaxation' stage), as shown in Fig. 2(a). The total number of steps is taken as 2000, equally distributed between the two stages. In our analysis, t_2 assumes a fixed value of 8s, while t_1 is variable. In Fig. 2(b), we display the Cauchy stress results for four different values of t_1: 4s, 2s, 1s and 0.1s. We observe significant rate dependency both on the elastic and plastic phases, with greater stiffness values on the cases with higher strain rates (i.e. smaller t_1), resulting in greater stress values at the end of the loading stage. On the other hand, during the relaxation stage, the final stress values tend to be lower for the higher strain rates, due to the greater plastic strains in these cases.

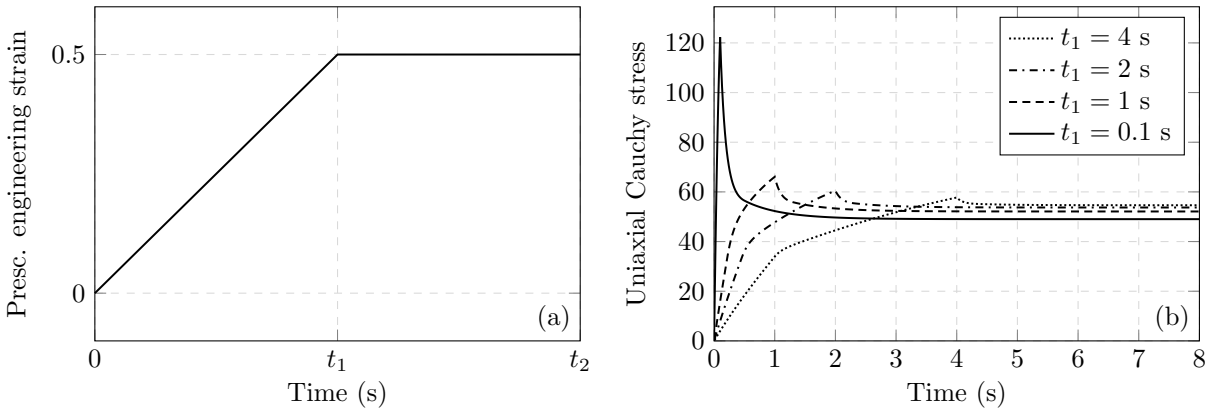

Figure 2. Uniaxial relaxation test. (a) Prescribed engineering strain over time and (b) Cauchy stress over time.

For the creep test, we apply prescribed compressive nominal stress, fixed at -100MPa up until the time instant t_1 ('loaded creep' stage), and fixed at 0 from t_1 to t_2 ('unloaded' stage), as shown in Fig. 3(a). The total number of steps is taken as 1000, equally distributed between the two stages. In our analysis, t_2 assumes a fixed value of 10s, while t_1 is variable. In Fig. 3(b), we display the engineering strain results for five different values of t_1: 5s, 2.5s, 1s, 0.1s and 0.01s. As expected, the engineering strain increases over the time during the loaded stage, consequently resulting in higher values for the cases with greater t_1. Accordingly, the plastic strain also increases with the time, resulting in higher residual strains during the unloaded stage. This behaviour, as well as the one in the relaxation case, is generally seen in experimental results of viscoelastic-viscoplastic materials (see, for instance, [3]), indicating that the present model can indeed properly represent such materials.

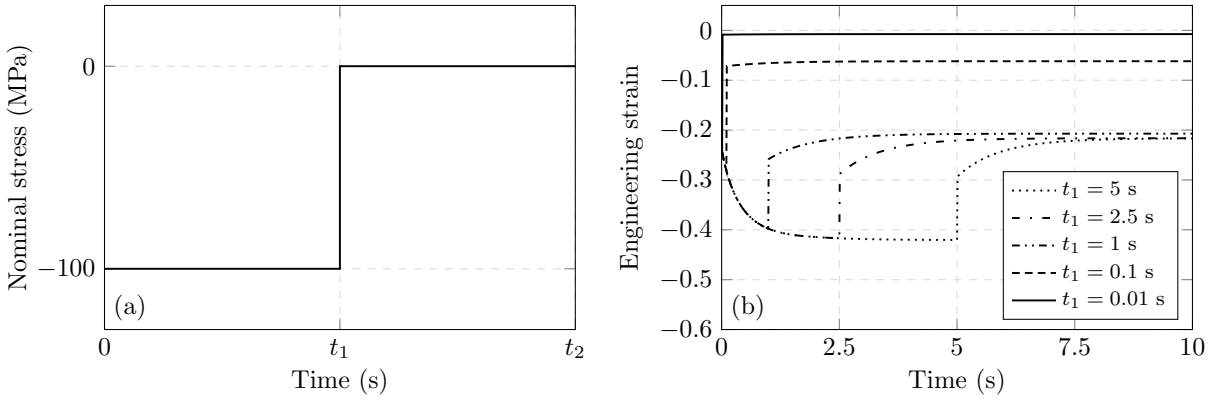

Figure 3. Uniaxial creep test. (a) Prescribed nominal stress over time and (b) engineering strain over time.

7 Partially loaded block

This example consists of a rectangular block subject to a partially applied compressive load, as shown in Fig. 4, with the material parameters from Table 1, and plane strain approximation. For the finite element application, we employ the geometrically nonlinear formulation described in [11, 17, 18], characterized by using positions as nodal parameters, instead of displacements, and a total Lagrangian description. For this example, we employ a 10-node triangular element with cubic approximation (T10). Due to the symmetry, only half of the geometry is discretized, with a mesh of 200 triangular elements and 961 nodes. In order to cover different strain and stress rates, the maximum analysis time t_1 is variable, with the total number of steps fixed as 10000.

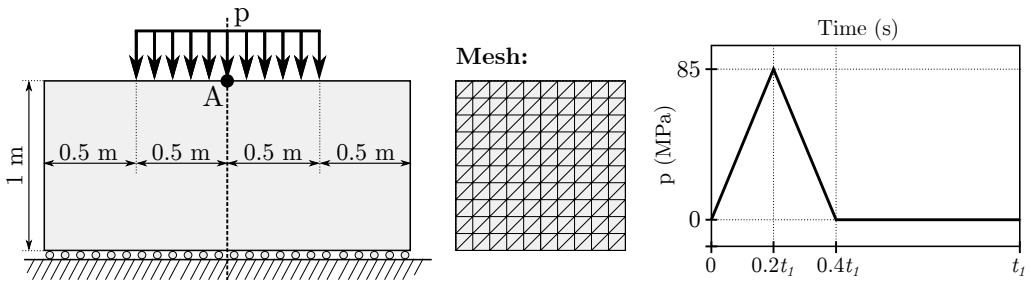

Figure 4. Geometry and mesh for the partially loaded block example

In the Fig. 5, we show the results of vertical displacement measured at point A, for different values of t_1. Again, we observe a increasing of stiffness values for the cases with higher load rates, resulting in smaller displacements. As expected, this affects not only the viscoelastic response, but also the viscoplastic. In particular, for the case with $t_1 = 0.5 \cdot 10^{-1}$s, the problem approaches a simple hyperelastic behaviour, with negligible residual displacement after the unloading stage. The evolution of displacements after the unloading is also negligible in the cases with lower rates (i.e. higher t_1 values), despite the residual displacement being higher, and can only be noticed in the cases with intermediate rates ($t_1 = 0.5 \cdot 10^1$s and $t_1 = 0.5 \cdot 10^2$s). In Fig. 6, we show the deformed configuration at the maximum load step (20% time percentage) and the final step (100% time percentage), for four different values of t_1, with vertical viscous deformation $(E_v)_{22}$ displayed in the colour map.

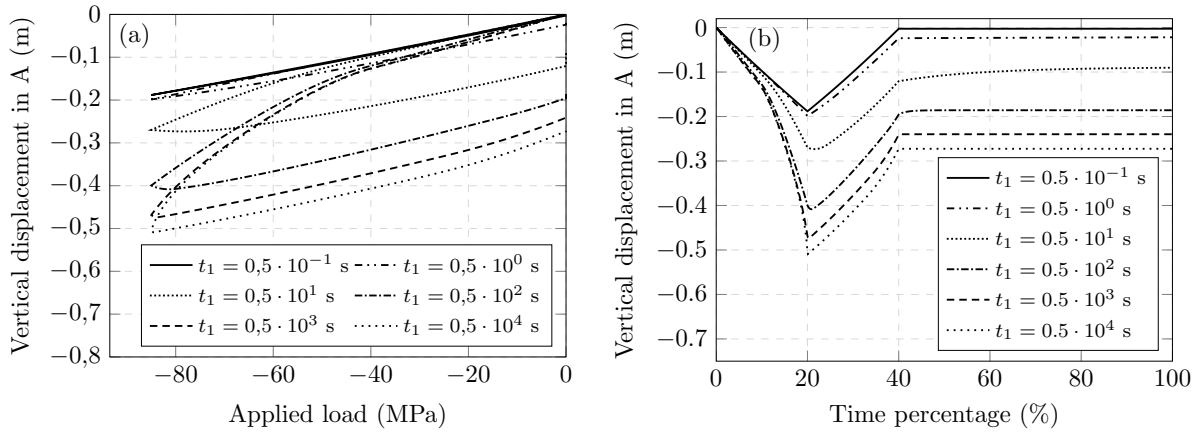

Figure 5. Graphs of (a) displacement by force and (b) displacement over time, for the partially loaded block example.

Following, we investigate the time-dependency of the property of inelastic incompressibility, with a convergence analysis of the plastic and viscous Jacobian errors. For this, we set $t_1 = 0.5 \cdot 10^4$s, using four different time discretizations, with Δt values of 2s, 1s, 0.5s and 0.25s. In Fig. 7 we show the maximum error on the plastic and viscous Jacobian for each of these cases, using a logarithmic scale. As can be seen, the errors are negligible for

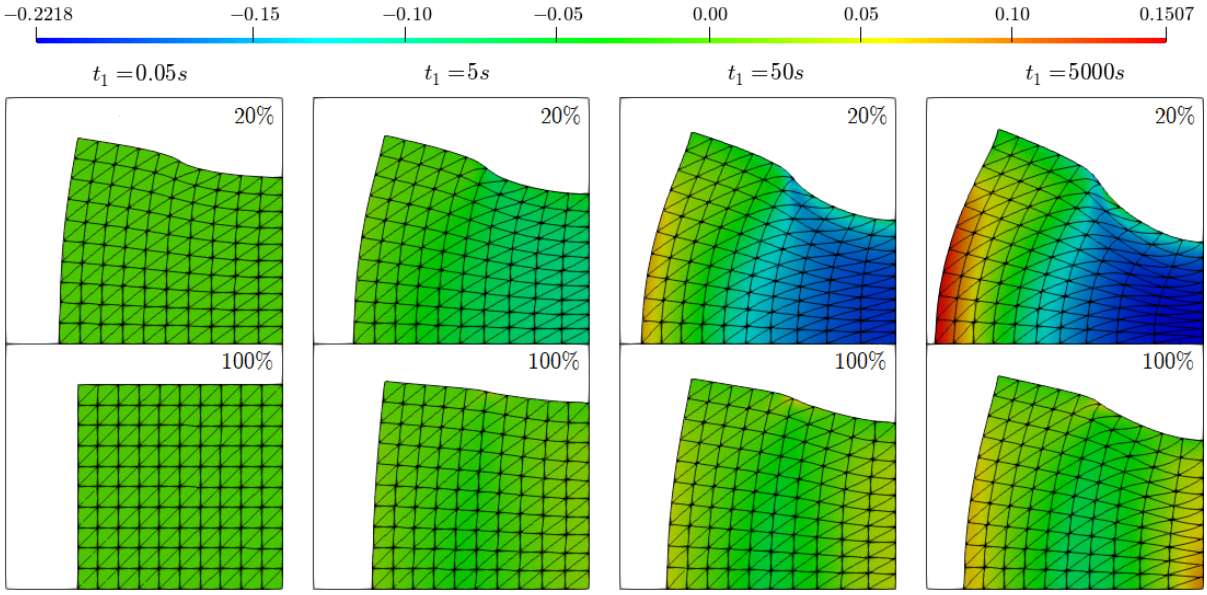

Figure 6. Deformed configuration of the partially loaded block example at 20% and 100% time percentage for four different load rates, with vertical viscous deformation $(E_v)_{22}$ displayed in colour map

practical purposes, and, furthermore, can be reduced by using smaller values of Δt. More precisely, the inclination of the lines in both graphs are approximately 1.149944643 and 1.023697852, respectively, indicating that both have a near first order convergence.

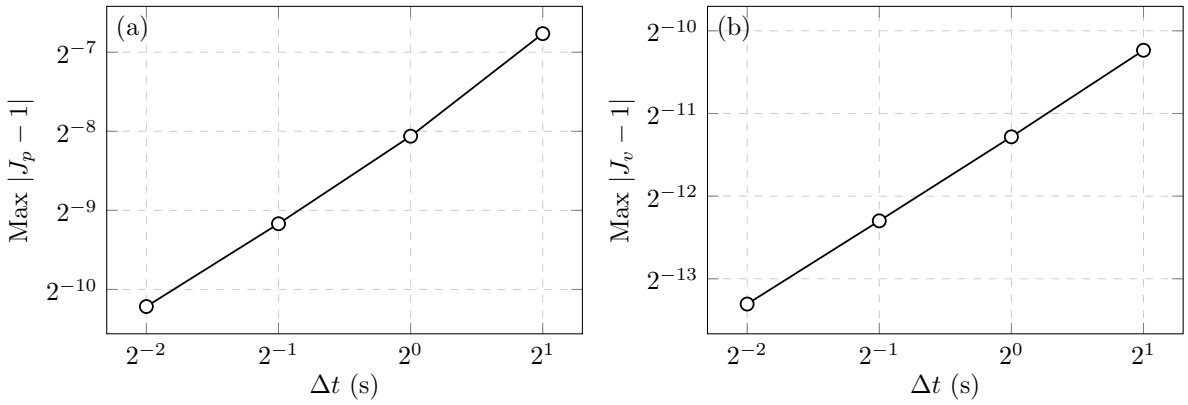

Figure 7. Convergence analysis for the (a) plastic Jacobian and (b) viscous Jacobian.

8 Conclusions

In this work, we proposed a thermodynamically-based viscoelastic-viscoplastic constitutive model applied to large strain problems. We began our analyses by showing the constitutive response of the model for simple uniaxial problems of relaxation and creep. The observed behaviour is consistent with the experimental results of viscoelastic-viscoplastic materials, such as polymers and asphalt. Following, we incorporated the proposed constitutive model to a nonlinear Finite Element framework, and applied it to a representative example of partially loaded cube. On this problem, we analysed the constitutive behaviour produced by monotonic loading-unloading under a wide range of load rates, and the property of inelastic incompressibility. For the latter, we concluded that the correct evaluation of inelastic Jacobians is indeed affected by the numerical implementation, particularly the time integration algorithm. However, the errors are negligible for practical purposes, and can be further reduced by refining the time discretization.

Acknowledgements. This study was financed in part by the *Coordenação de Aperfeiçoamento de Pessoal de Nível Superior – Brasil* (CAPES) – Finance Code 001 –, the Brazilian agency National Council for Scientific and Technological Development (CNPq) – grant 310482/2016-0 – , and the São Paulo Research Foundation (FAPESP) – Process Number 2018/23957-2. The authors would like to thank them for the financial support given to this research.

Authorship statement. The authors hereby confirm that they are the sole liable persons responsible for the authorship of this work, and that all material that has been herein included as part of the present paper is either the property (and authorship) of the authors, or has the permission of the owners to be included here.

References

[1] A. S. Khan and H. Zhang. Finite deformation of a polymer: Experiments and modeling. *International Journal of Plasticity*, vol. 17, pp. 1167–1188, 2001.

[2] N. Lammens, M. Kersemans, I. D. Baere, and W. V. Paepegem. On the visco-elasto-plastic response of additively manufactured polyamide-12 (pa-12) through selective laser sintering. *Polymer Testing*, vol. 57, pp. 149 – 155, 2017.

[3] M. K. Darabi, R. K. A. Al-Rub, E. A. Masad, C.-W. Huang, and D. N. Little. A thermo-viscoelastic–viscoplastic–viscodamage constitutive model for asphaltic materials. *International Journal of Solids and Structures*, vol. 48, n. 1, pp. 191 – 207, 2011.

[4] B. Nedjar. Frameworks for finite strain viscoelastic-plasticity based on multiplicative decompositions. part i: Continuum formulations. *Computer Methods in Applied Mechanics and Engineering*, vol. 191, n. 15, pp. 1541–1562, 2002a.

[5] B. Nedjar. Frameworks for finite strain viscoelastic-plasticity based on multiplicative decompositions. part ii: Computational aspects. *Computer Methods in Applied Mechanics and Engineering*, vol. 191, n. 15, pp. 1563–1593, 2002b.

[6] D. Perić and W. Dettmer. A computational model for generalized inelastic materials at finite strains combining elastic, viscoelastic and plastic material behaviour. *Engineering Computations: Int J for Computer-Aided Engineering*, vol. 20, pp. 768–787, 2003.

[7] D. W. Holmes, J. G. Loughran, and H. Suehrcke. Constitutive model for large strain deformation of semicrystalline polymers. *Mechanics of Time-Dependent Materials*, vol. 10, n. 4, pp. 281–313, 2006.

[8] E. Kröner. Allgemeine kontinuumstheorie der versetzungen und eigenspannungen. *Archive for Rational Mechanics and Analysis*, vol. 4, n. 4, pp. 273–334. cited By 23, 1960.

[9] E. H. Lee. Elastic-plastic deformation at finite strains. *Journal of Applied Mechanics*, vol. 36, n. 1, pp. 1–6. NUMISHEET2005 Conference, 1969.

[10] N. Huber and C. Tsakmakis. Finite deformation viscoelasticity laws. *Mechanics of Materials*, vol. 32, pp. 1–18, 2000.

[11] J. Pascon. High-order triangular finite elements applied to visco-hyperelastic materials under plane stress. *Journal of the Brazilian Society of Mechanical Sciences and Engineering*, vol. 40, pp. 40:535, 2018.

[12] P. Perzyna. Fundamental problems in viscoplasticity. volume 9 of *Advances in Applied Mechanics*, pp. 243 – 377. Elsevier, 1966.

[13] W. Dettmer and S. Reese. On the theoretical and numerical modelling of armstrong-frederick kinematic hardening in the finite strain regime. *Computer Methods in Applied Mechanics and Engineering*, vol. 193, n. 1, pp. 87 – 116, 2004.

[14] I. N. Vladimirov, M. P. Pietryga, and S. Reese. On the modelling of non-linear kinematic hardening at finite strains with application to springback – comparison of time integration algorithms. *International Journal for Numerical Methods in Engineering*, vol. 75, n. 1, pp. 1–28, 2008.

[15] O. M. Heeres, A. S. Suiker, and de R. Borst. A comparison between the perzyna viscoplastic model and the consistency viscoplastic model. *European Journal of Mechanics - A/Solids*, vol. 21, n. 1, pp. 1 – 12, 2002.

[16] J. J. Lemaitre. *Handbook of materials behavior models*. Academic Press, 2001.

[17] H. B. Coda and R. R. Paccola. A total-lagrangian position-based FEM applied to physical and geometrical nonlinear dynamics of plane frames including semi-rigid connections and progressive collapse. *Finite Elements in Analysis and Design*, vol. 91, pp. 1–15, 2014.

[18] J. Pascon and H. Coda. Large deformation analysis of elastoplastic homogeneous materials via high order tetrahedral finite elements. *Finite Elements in Analysis and Design*, vol. 76, pp. 21 – 38, 2013a.